Chapter 9

ELECTRON TRANSPORT DURING SOLAR FLARES

Jeongwoo Lee
Physics Department, New Jersey Institute of Technology, Newark, NJ 07102, U.S.A. *
leej@njit.edu

Abstract In this chapter we discuss microwave observation as a tool for investigating kinetic process of high energy electrons in solar flares. An ultimate goal of such studies is determination of electron evolution as a result of acceleration and transport in the presence of inhomogeneous magnetic field, and our focus is on why microwave radiation should be adequate for achieving this goal. The microwave studies devoted to such problems are briefly reviewed, and the main paradigms are expressed in simple formulations for so-called trap-and-precipitation systems. These formulations are then taken as a basis for organizing and illuminating contemporary ideas that recently emerged, including direct precipitation, various pitch angle scattering, and energy variation. The ideas enlarged from the discussions may guide the use of the FASR as an exceptional tool for solar flare study.

Keywords: acceleration of particles — Sun: flares — Sun: radio radiation — Sun: magnetic fields — radiation mechanisms: nonthermal

1. Introduction

Solar flares are an important example in the study of astrophysical particle acceleration, because they present a number of radiative characteristics indicative of kinetic processes of high energy particles in details unparalleled with other astronomical observations (Miller *et al.* 1997). As observational characteristics become known in increasing numbers, we, however, encounter an ambiguity as to whether the observed characteristic is directly due to acceleration or alternatively due to some transport effect (see Petrosian 1990). The ability to

*This work was supported by NASA grants NAG 5-10891 and NAG-11875

D.E. Gary and C.U. Keller (eds.), Solar and Space Weather Radiophysics, 179–202.

identify each of these two physical effects from observations therefore appears to be a key to further advancement in the study of kinetic processes in solar flares. During the last three decades, the problem of electron acceleration and transport has been discussed largely with Hard X Ray (HXR) observations (Aschwanden 2003) and partly with observations at microwaves (Bastian, Benz, & Gary 1998; Gary 2000) and other radio wavelengths (Wild & Smerd 1972; Dulk 1985). In this chapter we mainly discuss Microwave Radiation (MWR), as a tool for exploring the electron acceleration and transport processes during solar flares.

In 1966, Takakura & Kai formulated MWR spectral evolution as an electron transport problem for the first time, taking into account Coulomb collisions and synchrotron losses. Later several authors (Crannell *et al.* 1978; Cornell *et al.* 1984) found that lightcurves of MWR and HXR share an overall similarity, but MWR reaches its maximum in a delayed time and decays over an extended period. In a more systematic study, Lu & Petrosian (1988) found both short and relatively longer delays between 17 GHz and HXR, which they interpreted as due to transport and acceleration effects, respectively. Since then, further efforts have been made to interpret MWR observations using the ideas developed in HXR studies such as spectral hardening in the trapped electrons (Melrose & Brown 1976) and energy dependent time delay under Coulomb collisions (Bai & Ramaty 1979). Along this line, Melnikov (1990; 1994) presented for the first time microwave spectral evolution under Coulomb collisions, using Melrose & Brown's (1976) model. Similar studies followed, to account for the frequency-dependent time delays between MWR peaks as well as the relative delay of MWR to HXR peaks within the physics of Coulomb collisions (Bruggman *et al.* 1994; Bastian & Aschwanden 1997; Melnikov & Magun 1998; Silva, Wang, & Gary 2000).

Besides the time correlations, some authors compared MWR flux with proton flux (Bai 1982; Kai, Kosugi & Nitta 1985; Daibog *et al.* 1989; Melnikov *et al.* 1991; Daibog, Melnikov & Stolpovskii 1993), and with HXR fluxes (Kosugi, Dennis & Kai 1988; Melnikov 1990; 1994). They commonly found that extended (gradual) flares tend to show excess MWR flux, implying accumulation of electrons in a trap. Kai (1985) proposed that MWR is emitted by directly precipitating electrons in an attempt to resolve the problem of inconsistent numbers of electrons deduced from HXR and from MWR. Klein, Trottet, & Magun (1986) showed that use of a common injection function for both HXR and MWR can help in resolving the number problem too. The understanding that has emerged from these correlative studies is that MWR and HXR electrons share a common origin but, depending on whether they are emitted by the trapped or precipitating electrons, different fluxes and numbers may result.

While the above studies mainly deal with the effect of Coulomb collisions on the electron energy, more recent studies add the effects of Coulomb collisions on electron pitch angles together with magnetic mirroring. Lee & Gary (2000) and Lee, Gary & Shibasaki (2000) have analyzed a burst of which spectral evolution is due to not only collisional energy loss but pitch angle diffusion. Kundu *et al.* (2001a) studied time profiles of simple impulsive MWR bursts in comparison with HXR lightcurves, and explained the relative difference within the trap-and-precipitation model (Melrose & Brown 1976). Lee *et al.* (2002) studied an impulsive MWR event with rather long tail, using direct precipitation and a time-dependent injection spectrum inferred from HXR.

Transport effects have also been discussed with imaging observations. VLA observations have shown that in many flares the MWR source starts at the loop top and moves apart towards footpoints, which could be regarded as direct indication of the main energy release and subsequent propagation (see review by Marsh & Hurford 1982). Petrosian (1982) presented a more general consideration for the loop-top MWR source, including the radiative efficiency and particle kinetics. Holman *et al.* (1982) proposed that a loop top source and its expansion (Marsh & Hurford 1980) represent an instantaneous trap of the high energy electrons and subsequent pitch angle diffusion. Kundu *et al.* (1995) observed an asymmetric pair of MWR sources and interpreted it as due to asymmetric precipitation of nonthermal electrons under weak diffusion. The asymmetric MWR source presented in Lee, Gary & Shibasaki (2000) and Lee & Gary (2000) was also interpreted as due to magnetic mirroring under weak pitch angle diffusion. Melnikov, Shibasaki & Reznikova (2002, 2003) studied MWR loop-top sources at 17 and 34 GHz, which they found to represent an actual concentration of electrons rather than a radiative transfer effect.

Another type of imaging study has been made by Hanaoka (1996; 1997), Nishio *et al.* (1997), and Kundu *et al.* (2001b) using Nobeyama 17 GHz imaging data together with HXR images from the *Yohkoh* satellite, who argue for reconnection of interacting loops, inferred from their multiple footpoints. Lee *et al.* (2003) found spatial coincidence of the MWR sources with the magnetic separatrix inferred from a magnetogram and Hα ribbons in an impulsive flare. These studies have suggested some gross properties of magnetic reconnection, which is responsible for the particle acceleration, and resulting propagation away from the acceleration site.

In summary, we see that the early spectral/time studies suggested that MWR and HXR are related to trap-and-precipitation, respectively, and this can be known from the electron energy variation. However some of the recent imaging observations (Kundu *et al.* 2001a, b; Lee *et al.* 2002; Melnikov *et al.* 2002; 2003) suggest that electron pitch angles and inhomogeneous magnetic fields are also important elements in the transport problem. In the rest of this chapter, we

will discuss key issues in electron acceleration and transport within the latter paradigm.

2. The Formulations

Let us present a simplest possible formulation with which we can illustrate the recent and past picture of trap-and-precipitation in a unified fashion. Suppose electrons are injected into a trap by the quantity Q and leave the trap at a rate ν, in which case the Fokker-Planck equation will be in the form:

$$\frac{\partial N}{\partial t} = [\dots] - \nu N + Q \ ,$$

where $[\dots]$ should include all the variations in momentum and space. The solution to this equation takes a form of $N = K \otimes Q$, where the kernel function K accommodates all the terms in the right hand side except the injection. Our problem is therefore how to deconvolve Q from the resulting electron distribution function N obtained from the observed radiation. In general all of these quantities N, Q, and K involve time, energy and pitch angle as arguments, and not only the solution but even the formulation is not always expressed in a convenient closed form. Here we consider a simple case where all the terms in $[\dots]$ can be ignored, which corresponds to a collisionless trap where there is no loss of particles other than that due to escape (νN) and its pitch angle-dependence is implicitly handled. In this case the kernel function is simply an exponential function, and solution for trapped electrons is in the form $N = \int_0^t e^{-\nu(t-t')} Q(E,t') dt'$, where the transport effect is solely described by the property of the escape rate ν (as used in Aschwanden 1998; Kundu *et al.* 2001a; Lee *et al.* 2002).

2.1 Trap-and-precipitation

The above N alone provides electrons in a perfect trap, with ν, representing some loss rate. Melrose & Brown (1975) presented a model in which the trap region (thin target) is connected to a precipitating region (thick target) and therefore the escape rate ν is set as the precipitation rate which in turn becomes an injection rate into the thick target region. To express this idea under our simplifying assumption given above, we have

$$\begin{array}{rcl} N & = & \int_0^t e^{-\nu(t-t')} Q(E,t') dt' \\ \dot{n} & = & \nu N(E,t) \end{array} \ , \qquad (9.1)$$

where N is the number density in the trapped electrons (thin target) and $\dot{n}$ is injection rate into the thick target region. In this model, ν is the central quantity whose magnitude and energy dependence governs the lives of the

trapped electrons (N) and precipitating electrons ($\dot{n}$). As a major advantage, the N and $\dot{n}$, which are believed to be responsible for MWR and thick-target HXR, respectively, can be related to each other via the single physical effect of pitch angle scattering. As a limitation, however, the model predicts that the time evolution of the HXR electrons ($\sim \dot{n}$) should be well correlated with that of the MWR electrons ($\sim N$), whereas HXR often appear with a shorter timescale than the MWR.

2.2 Trap, bypass, and precipitation

As an important step forward, Aschwanden (1998) included another component in to the formulation, a population associated with direct precipitation ("by-passing the trap" in other words). To illustrate this idea, we split the injected particles Q into two parts, according to whether the initial pitch angles are greater or smaller than the loss-cone angle, i.e., $Q(\phi^+)$ and $Q(\phi^-)$, where $\phi^+(\phi^-)$ represents the electron pitch angles greater (smaller) than the loss-cone angle, ϕ_L (cf. MacKinnon 1991). The loss-cone angle is set by the magnetic mirror ratio of the flaring loop, $\phi_L = \sin^{-1}(B_1/B_2)$, with B_1 and B_2 representing the magnetic field strength at the loop top and a footpoint, respectively. Since the particles with ϕ^- can *directly* precipitate without being trapped, (9.1) should be modified to the following form:

$$\begin{array}{rcl} N & = & \int_0^t e^{-\nu(t-t')} Q(E, \phi^+, t') dt' \\ \dot{n} & = & Q(E, \phi^-, t) \; + \; \nu N \end{array} \quad . \tag{9.2}$$

Note that (9.2) will reduce to (9.1) in the limit of $\phi_L \rightarrow 0$, i.e. all particles are initially trapped and then are able to precipitate. We can thus say that (9.1) is valid to the extent that ϕ_L can be ignored. Another limit in which both equations approach to each other is at $\nu \rightarrow \infty$. In this case $N \rightarrow 0$ and $\dot{n} \rightarrow Q$, which means that observed radiation is a direct consequence of acceleration with no transport effect. These two cases represent the entirely trapped (transport-dominated) and entirely untrapped (acceleration-dominated) cases, respectively.

Equation (9.2) shows, on a minimum basis, how the magnetic field and pitch angle distribution comes into the context of trap-and-precipitation. Under this model, we can treat the following issues: (1) The injection function can, at least in the portion $Q(\phi^-)$, be subject directly to observations rather than treated as a free parameter. (2) The precipitating population can behave differently from the trapped one if the bypassing component $Q(\phi^-)$ dominates over the secondary precipitation νN. As a result, we can have an impulsive HXR and more extended MWR in an event. (3) The finite magnetic field comes into the context, at a minimum, in the form of mirror ratio. (4) Since N and $\dot{n}$ can have different time behaviors, the combination of these two terms can produce various

types of MWR lightcurves, especially, a burst with impulsive rise and extended decay. In the next section we will apply these ideas to actual observational data.

3. Electron Trapping And Precipitation

In this section, we consider various classes of MWR activities as evidence of the trap-and-precipitation system as formulated above.

3.1 Simple bursts

When a flare produces a single or small number of bursts in HXR and is accompanied by more extended MWR emission, we expect that the HXR would be a result of direct precipitation and thus would represent injection, while MWR will be given by a convolution of the HXR profile with the kernel function. Such events were recently studied by Kundu *et al.* (2001a) and Lee *et al.* (2002). We show a result presented by Kundu *et al.* (2001a) in Figure 9.1. In the figure, the authors compare the NoRH lightcurves at 17 and 34 GHz with HXR from HXT/Yohkoh. Both HXR and MWR has the same initial rise and the core part of the impulsive peak is similar in both radiations. Such coincidence (excluding the time-of-flight effect as studied by Aschwanden and his colleagues) can be taken as evidence for direct precipitation. Then the extended tail of the MWR is interpreted as due to trapped electrons. Kundu *et al.* reproduced its time behaviors using a convolution of HXR which has been taken as injection. In our notation, this is to say that the HXR represents the direct precipitation into a thick target $\sim Q(\phi^-)$, and the MWR is contributed by both trapped and directly precipitating electrons $\sim K \otimes Q(\phi^+) + Q(\phi^-)\,\ell/u$, where ℓ/u is the transit time for an electron of speed u in a loop of length ℓ.

The distinction between injection and trapping was made possible here because the HXR emission is dominated by thick target emission while MWR is from both components. MWR responds to both components because of its greater sensitivity to energetic electrons, whether they are located in the dense chromosphere or tenuous corona. Therefore the relative difference between MWR and HXR serves as a measure of transport effects. A similar conclusion is presented by Lee *et al.* (2002) in which a HXR spectrum is used to derive an injection function in a time dependent spectrum, and this is used to reproduce MWR bursts, taking into account full radiative transfer as electrons pass through an inhomogeneous magnetic loop.

3.2 Trap or precipitation?

Many solar flares show multiple peaks in MWR and HXR, in which case there may form a smooth envelope underneath the impulsive peaks. In this case, the trapping and direct precipitation could be attributed to the smooth envelope and superposed pulses, respectively. The individual MWR peaks

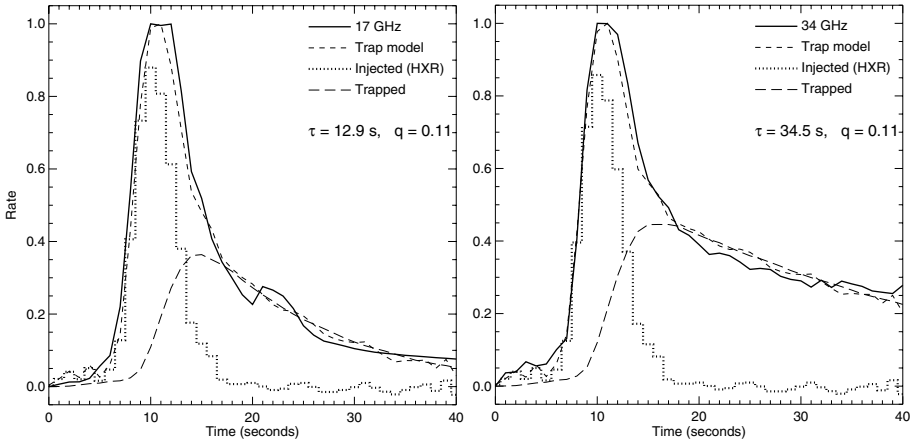

Figure 9.1. Comparison of the radio time profiles for the event on 1998 June 13 for (left) 17 GHz and (right) 34 GHz with a trap model (short-dashed line) derived using the Yohkoh/HXT 53–93 keV hard X-ray time profile (dotted histogram) as an injection function. The radio time profile is modeled as the sum of a component identical to the hard X-ray time profile (the injection function) and a trapped component (long-dashed line) derived by integrating over the injection function convolved with an exponential kernel function. τ and q denoted in this figure are respectively equivalent to ν^{-1} and $Q(\phi^-)/Q(\phi^+)$ in our notation. (From Kundu *et al.* 2001*a*).

themselves may not be much delayed or extended compared with those of HXR, but the presence of the underlying envelope in MWR may obscure the similarity expected between the two radiations. We show such an example in Figure 9.2. The solid lines are MWR and HXR lightcurves, and the dashed lines are fit by eye to the background envelope. The result difference profiles give a set of short pulses. Since they show peak-to-peak correspondence between two radiations, we regard them as representing the direct precipitation ($\sim Q(\phi^-)$) during the event. As we regard the smooth envelope as the trapped population, we require it to be reproduced by convolution of the net impulsive peaks with some kernel function. Although the exact account of this calculation depends on how one sets the background, we do indeed find a rough fit to the observed HXR envelope at $\nu = 1.2 \times 10^{-2}$ s^{-1}. The MWR envelope is more extended and the fit is made at a much lower value of $\nu = 5.1 \times 10^{-3}$ s^{-1}, implying a longer lifetime of electrons compared with the HXR case.

The two different values of ν for MWR and HXR could simply reflect an energy dependence of the precipitation rate, given the expectation that the MWR and HXR are contributed by electrons with different energies. It is also possible that the effective emitting region for HXR has different physical parameters than that for MWR or that the envelopes in HXR and MWR represent the secondary

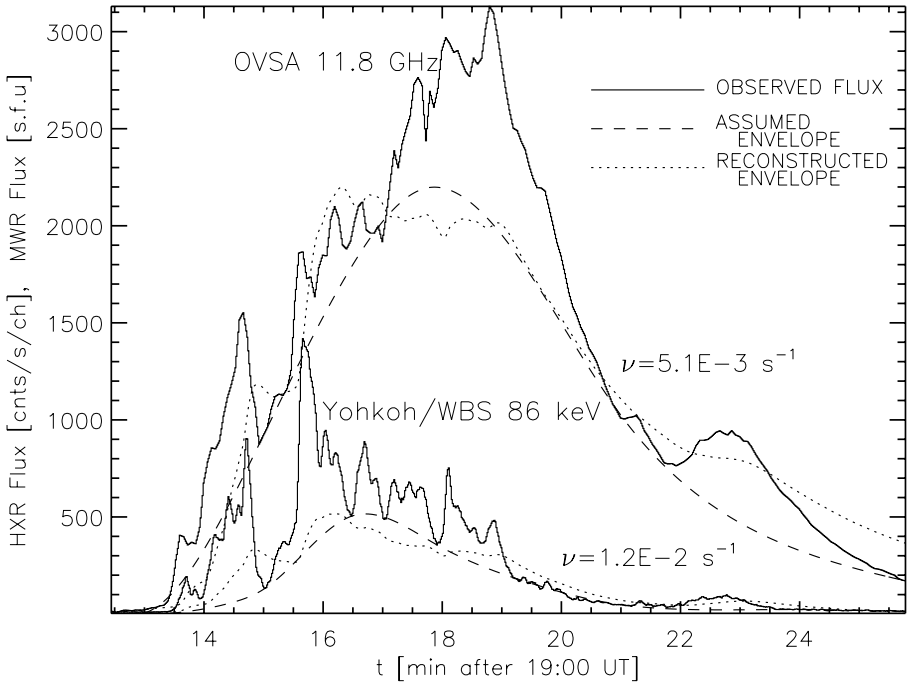

Figure 9.2. An impulsive burst that occurred on 2001 April 6. The solid lines are lightcurves at MWR at 11.8 GHz and HXR 86 KeV from Yohkoh/WBS. The dashed lines are the envelope of each curve obtained by smoothly connecting the local minima of the curves. The fluctuation above the envelope shows a peak-to-peak correspondence and is regarded as due to direct precipitation. This is then convolved with a kernel function in an attempt to self-consistently reproduce the envelope, shown as dotted lines.

precipitation, νN, and trapped electrons, N, respectively. With the temporal profile alone, we have no way to distinguish among these or other possibilities. However, HXT/*Yohkoh* imaging data available for this event showed that the HXR sources appear on the footpoints, by which we could conclude that the smooth HXR envelope is due to secondary precipitation while the MWR envelope is due to the trapped component. In this case also, the relative difference between MWR and HXR serves as a measure of trapping.

3.3 Extended and evolving trap

Large flares usually show temporally extended MWR activity, as do the accompanying soft X-rays and HXRs. Naively speaking, a large flare is powered by a larger amount of energy, and therefore activity can be extended in time. Alternatively the extended activity may be a result of long term trapping associ-

ated with the large physical extent of such a flare. This leads to a long standing question as to whether the extended activity is due to prolonged acceleration or efficient trapping, in other words, whether it is due to a longer τ_a or smaller ν.

An example of extended MWR bursts, the 1991 March 22 flare, is shown in Figure 9.3. The left panel shows the MWR lightcurves at multiple frequencies and the right panel, MWR spectra at selected times (symbols) together with a model fit (solid lines). Note that the extent of the activity is not equally long at all frequencies, but varies rapidly across frequencies. Based on the idea presented in the previous section, we speculate that the short-period activity at the highest frequency (18 GHz) represent the injection-related component ($\sim Q(\phi^-)\,\ell/u$) and longer period activity toward lower frequencies represent the more extended trapped component ($\sim N$). This then means that the extended activity in this event is not due to injection (which was impulsive) but due to efficient trapping, i.e., $\tau_a \ll \nu^{-1}$, where τ_a is the timescale for acceleration. Such a good trap condition may be realized simply because the ambient density in the coronal magnetic loop may be very low (for Coulomb collisions) or the mirror ratio may be high so that ϕ_L is small, or both.

We draw further attention to the frequency-dependence of the MWR activity. If Coulomb collisions dominated, and if the MWR frequency is simply proportional to the electron energy, the flux at a high frequency should have been longer than that at a low frequency, as opposed to the observation. Lee, Gary & Zirin (1994) made a model to fit such a spectral variation as shown in the right panels in Figure 9.3, in which the MWR source at the maximum phase spans the entire loop encompassing highly inhomogeneous magnetic fields, and then the trap gradually shrinks to a smaller region with weaker fields, i.e., the loop top. In such a model, the high frequency flux has short duration because it is emitted by directly precipitating electrons that are passing through the strong magnetic fields near the footpoints, and the gradual decay toward lower frequencies is, in fact, due to *harder* electrons surviving longer in the loop top. This type of burst demonstrates how significant the magnetic inhomogeneity can be to the evolution of MWR in a solar flare.

3.4 Trap without precipitation

In some events the correlation between MWR and HXR is so poor that we are puzzled about the common origin for MWRs and HXRs. A good example can be found in the famous Bastille Day flare as shown in Figure 9.4. In the top panel we compare the HXR and MWR lightcurves and in the bottom two panels, EUV images at 195 Å from Transition Region and Coronal Explorer (TRACE) before and after the impulsive phase. The HXR reached its maximum at t_1 and then diminished whereas the MWR has multiple peaks remaining strong throughout the flare. This temporal behavior differs from that shown in Figure 9.2 in

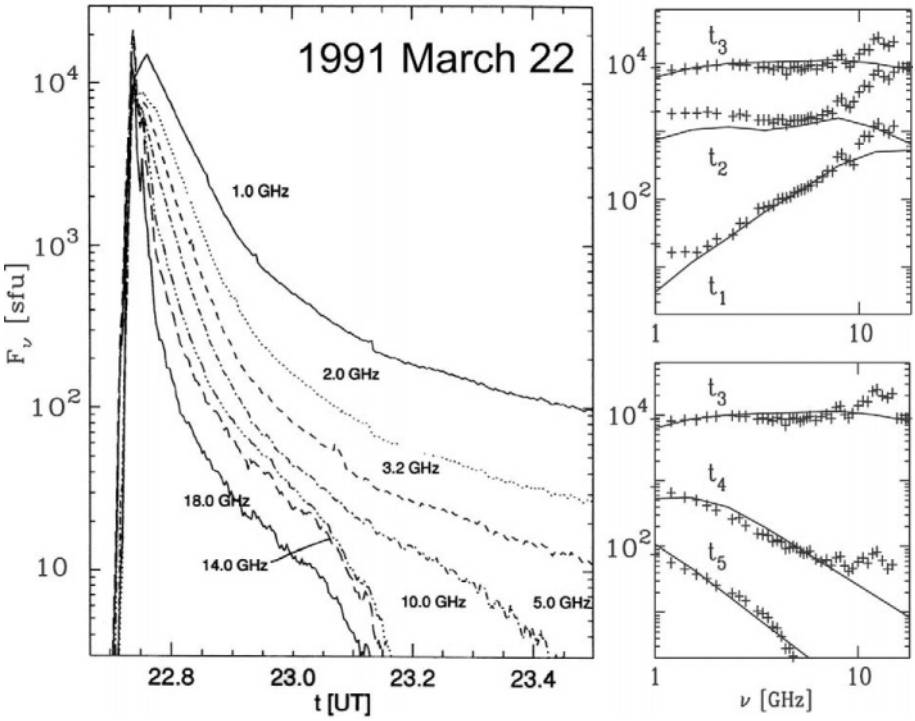

Figure 9.3. MWR bursts indicative of long-term trapping. In the leftmost panel, the 1991 March 22 flare shows an impulsive rise and extended decay, but with an obvious frequency-dependence. The right panels show MWR spectra at selected times (symbols) and a model fit (solid lines). $t_1 - t_5$ respectively refer to 22:43:20, 43:50, 44:10, 55:00, and 23:30:00 UT. The model assumes gradual shrinkage of the electron trap into smaller regions centered at the loop top, together with softening of the electrons in the decay.

that there is no HXR counterpart after t_1. It is also different from that in Figure 9.3 in that the continued MWR activity indicates multiple occurrences of additional acceleration rather than just efficient trapping. Aschwanden & Alexander (2001) had shown that the HXR peak (which is taken as evidence of precipitation in this chapter) is accompanied by soft X rays and EUV in gradually delayed time profiles, indicative of energy cascade from 30 MK to 1 MK. The MWR electrons therefore participate in this energy transfer to low atmosphere only at time t_1 but not afterwards, $t_{2,3,\ldots}$.

Such decoupling of MWR from other (precipitation-oriented) radiations is expected, within the current framework of (9.2), when either $\phi_L(t)$ gets smaller or $Q(\phi, t)$ becomes more anisotropic at times $\{t_1, t_2, \ldots\}$. The former can happen as a result of the loop rising with the same footpoints (or some magnetic restructuring) so that the magnetic mirroring force will increase, so that a larger

fraction of particles return back to the coronal trap. We find some clue for the magnetic field change in the TRACE EUV loops shown in the bottom panels. The bright features in the left panel are thought to be low-lying magnetic loops in an arcade, which grow outward after the flare to form the newly formed, relaxed loops shown in the right panel. Alternatively the rapid drop of precipitation could be due to a change in the ratio of the injected electrons within or outside of loss cone, $Q(\phi^+)/Q(\phi^-)$, which was moderate at t_1 but could have increased at $t_{2,3,...}$ by a large factor. This could therefore imply that the electron acceleration mechanism had changed so as to produce more electrons with a perpendicular momentum distribution (see §4.3). Also in this case, the electron loss in the coronal trap would not be due to precipitation but some other mechanism. An appropriate loss mechanism may be escape associated with the upward ejecta or propagation into interplanetary space.

To conclude this section, the framework of trapped and directly precipitating electrons such as (9.2) leads us to a physical interpretation of a variety of MWR and HXR lightcurves. However, quantitative assessment of the similarities and differences requires a knowledge of the electron pitch angle and magnetic field, ideally to be deduced from observations.

4. Electron Pitch Angle Variation

We have thus far discussed the role of the initial electron pitch angle distribution, $Q(\phi)$, in the evolution of the electrons in a trap-and-precipitation system (the evolution of N and $\dot{n}$). Changes in pitch angle during transport can also significantly influence the evolution of N and $\dot{n}$. In many studies, the electron pitch angle diffusion due to scattering has been directly related to the precipitation rate, ν. We, however, present in this section an alternative view that stronger pitch angle diffusion does not necessarily imply more efficient precipitation. Rather, we show that relating the electron pitch angle diffusion to the magnetic field loop structure leads to an independent tool for studying the acceleration and transport characteristics.

4.1 Weak diffusion

Weak pitch angle diffusion has been defined as the condition in which the loss cone is empty. As a result the loss cone size has not been considered a factor in the precipitation and the precipitation is expected to increase in proportion to the scattering rate. However, such an assumption overlooks the fact that at a given scattering rate a large loss cone is more difficult to fill compared to a small loss cone. Also, the scattering rate itself should depend on pitch angle, which varies along the electron motion according to the ambient magnetic field, under conservation of the magnetic moment (first adiabatic invariant) $\mu_\perp^2/2B$

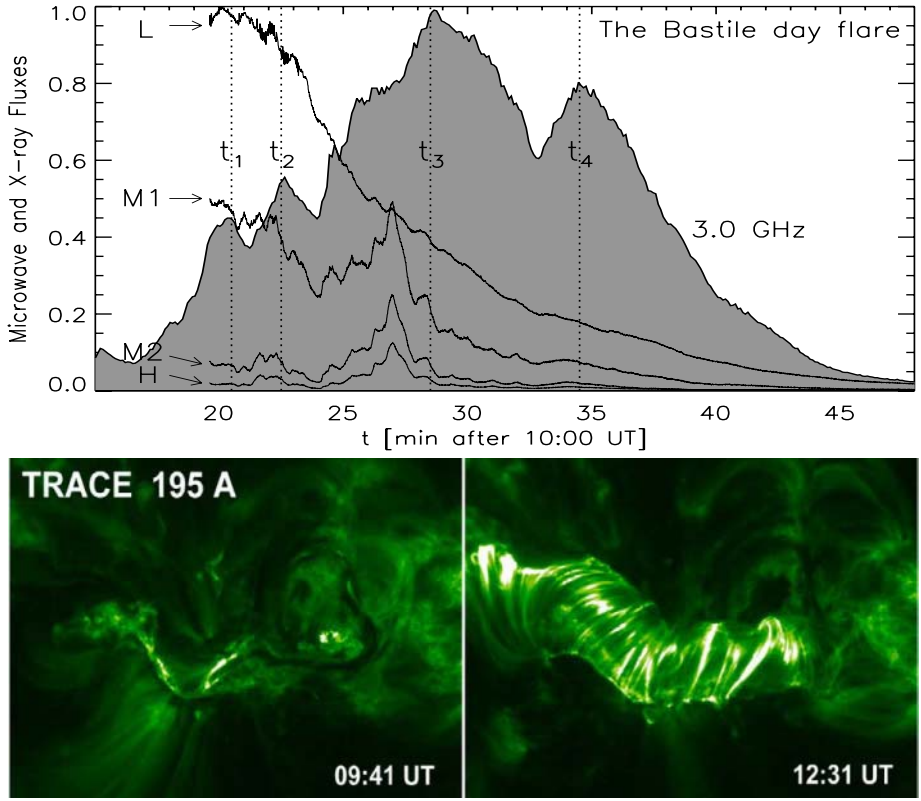

Figure 9.4. The top panel shows MWR and HXR lightcurves during the Bastille Day flare on 2000 July 14. The HXR lightcurves are from *Yohkoh* HXT at four energy channels, L, M1, M2, and H, and the 3.0 GHz MWR flux is from Ondrejov Solar Radio Telescope shown as the filled curve. Note the poor correlation between MWR and HXR lightcurves. The bottom panels show closeup views of the magnetic loops in the active region before and after the flare, as observed in 195 Å images obtained with the TRACE spacecraft.

(Melrose 1980). For these two reasons, pitch angle scattering even under weak diffusion cannot entirely be free from the magnetic field (see Lee & Gary 2000). The term weak diffusion has also been used to refer to a case where Coulomb collisions dominate, in the sense that Coulomb collisions always exist and any other scattering mechanism, if added, will make the scattering no longer weak. In this case the precipitation is given by the electron deflection time so that $\nu \approx 10\, n_9 E^{-3/2}\ \mathrm{s}^{-1}$ where E is in units of keV and n_9 is the ambient electron density in $10^9\ \mathrm{cm}^{-3}$ (Trubnikov 1965; Spitzer 1967). A comprehensive review and result of analysis that leads to a diagnostic of the trap density can be found in Aschwanden *et al.* (1997).

In an alternative, but perhaps more insightful, approach to reveal the presence of weak diffusion, Melrose & White (1979) suggested that spatial morphology of MWR could be asymmetric under weak diffusion because of asymmetric magnetic mirroring. Kundu *et al.* (1995) found an asymmetric spatial distribution of MWR sources and explained the observation within this context (see also Sakao 1995). Lee, Gary & Shibasaki (2000) and Lee & Gary (2000) reported an asymmetric MWR source in a magnetic loop, which is reproduced in Figure 9.5. The top panel shows that one of the double MWR sources is found at a footpoint and the other MWR source is some distance above the conjugate footpoint. Since the latter footpoint has stronger field, the asymmetric MWR source positions along the loop implies there are regions where electrons do not have access because of magnetic mirroring. The bottom panels show MWR spectral hardening during the decay phase, which indicates the influence of Coulomb collisions on the electron energy distribution. The theoretical modeling becomes more complicated in this case, since pitch angle and magnetic field inhomogeneity needs to be taken into account. Through a simplified simulation including electron pitch angles and a specific magnetic field structure of the loop, Lee & Gary (2000) found that a model fit to the observed spectral variation required an anisotropic pitch angle distribution in the injected electrons. Not only does the MWR spectrum show great sensitivity to the electron pitch angle distribution, but also the slow changes in the collisionless coronal trap. This allowed Lee & Gary (2000) to deduce the pitch angle distribution of the initial injection. This underscores the importance of MWR observations for the study of the properties of the coronal population, including pitch angle distributions.

4.2 Intermediate diffusion

In contrast to weak diffusion, Melrose & Brown (1975) defined the case of the loss cone being filled with scattered particles as "strong" diffusion. We shall instead call this "intermediate" diffusion to save the term "strong" diffusion for another case to be discussed in the next section (see Bespalov, Zaitsev & Stepanov 1991). If the loss cone is continually refilled, the rate of precipitation will be limited by the size of the loss cone, and is expressed as $\nu = \alpha_0^2 u/2\ell$, where α_0 is the loss-cone angle (Kennel 1969). The scattering rate is thus proportional to u (or $E^{1/2}$) independent of the scattering mechanism. While weak diffusion offers a number of interesting spatial structures associated with magnetic mirroring, intermediate diffusion would erase any such features by quickly isotropizing the electron momenta, and the whole loop is evenly occupied by the electrons. As a result, the spatially-averaged Fokker-Planck solution is appropriate in this case.

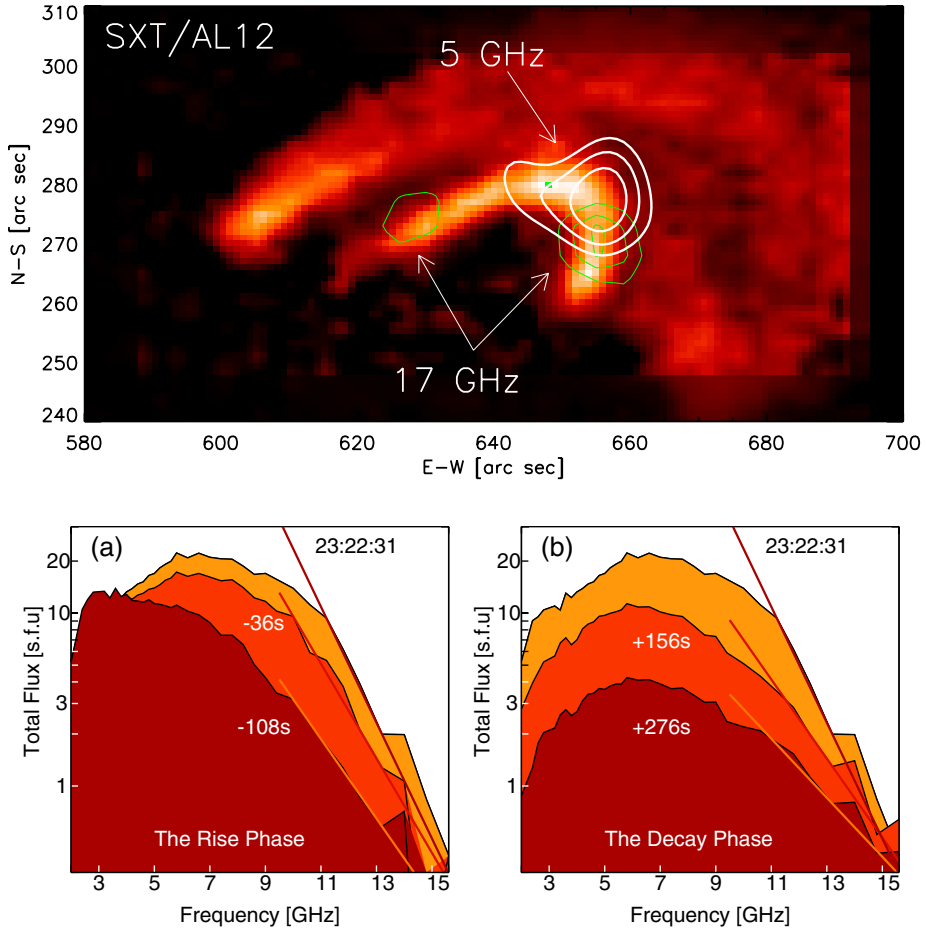

Figure 9.5. MWR maps and spectra obtained for the 1993 June 3 flare. Top: Radio intensity peaks (contours) on top of a soft X-ray image from a filtered *Yohkoh* SXT/AL12 at 23:29 UT. Contours are 80% to 99% of the maximum intensities: 1.8×10^7 K at 5 GHz and 1.2×10^5 K at 17 GHz, respectively. Bottom: Spectral variation in the microwave total power during (a) the rise and (b) the decay phases, at five selected times relative to the time of the maximum flux (23:22:31 UT). The straight lines are guide lines for spectral slope at the corresponding times. (From Lee & Gary 2000)

Figure 9.6 shows a model fit to the MWR fluxes during the 1999 August 20 flare (Lee *et al.* 2002) which led the authors to argue for intermediate diffusion. The OVSA visibility implied a large loop ($\ell \approx 1.4 \times 10^5$ km) entirely filled with accelerated electrons. Since morphology is of little help in the intermediate

diffusion case, the only way to know which pitch angle scattering scenario applies to this flare was to check the energy dependence of the precipitation rate. The authors compared the model predictions made under various energy dependencies with the MWR flux variation with frequency to find that the assumption of $\nu \sim E^{1/2}$ (case (b) in the figure) is the most appropriate. The MWR flux decays only slowly and the loss cone is found to be as small as $\alpha_0 \approx 4.3^\circ$. Thus in spite of the fact that it is not a weak diffusion case, the actual precipitation rate is very low. This is an example in which highly efficient pitch angle diffusion does not imply a high efficiency of precipitation. In retrospect, intermediate diffusion pertains in this event because the loss cone is small and can be easily filled, leading to the precipitation rate becoming independent of the scattering mechanism.

4.3 Strong diffusion

In the above case of "intermediate" diffusion, the precipitation rate depends on the whole loop length, implying that the scattered particles still remember the whole dimension of the loop at least over a few bounce times. Bespalov, Zaitsev & Stepanov (1991) defined another regime for pitch angle scattering as "strong" in which the scattering, for instance, due to the presence of enhanced turbulence, is so strong as to alter pitch angles so quickly that the mean free path is much shorter than the loop length. In this case, defining a loss cone is not meaningful and the electrons are effectively trapped within the scattering source. This is another example for which pitch angle diffusion and precipitation may be two independent, unrelated effects. An important aspect of this strong diffusion is that the region of such strong turbulence, if localized on a flaring loop, could give clues to the spatial location of the acceleration site and properties of the acceleration mechanism. Just as loop-top HXR sources (Masuda *et al.* 1994) have been much debated, the loop-top MWR source has also been a mystery considering the strong dependence of MWR emissivity on magnetic field strength. If the entire loop is optically thick, we may then expect the highest effective temperature of MWR to occur at the loop-top, because that is the location of the lowest field strengths, which are associated with the highest harmonics at a given frequency. This is demonstrated in several flare loop models (Alissandrakis & Preka-Papadema 1984; Klein & Trottet 1984; Lee *et al.* 1994). However if the loop-top source is optically thin, a looptop brightening implies an actual concentration of electrons at the position rather than an apparent radiative effect.

In Figure 9.7 we show an example of a loop top source from NoRH observations (Melnikov, Shibasaki & Reznikova 2003) at two frequencies. It is apparent from the figure that the 34 GHz image outlines a loop over an active

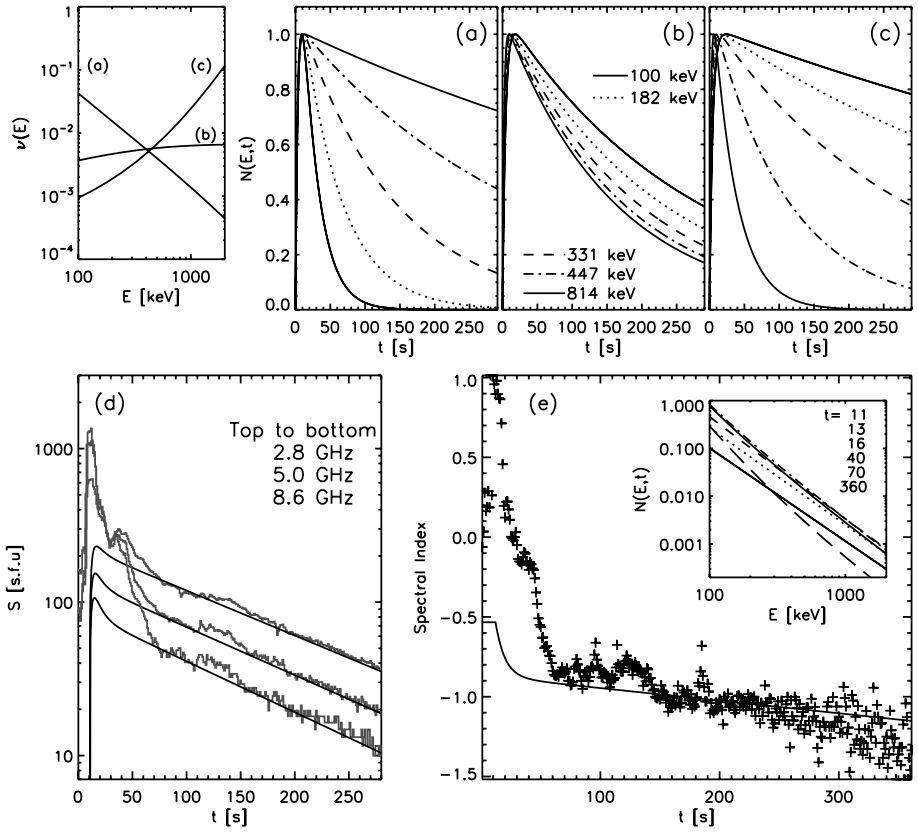

Figure 9.6. The 1999 August 20 flare as a case of intermediate pitch angle diffusion. The top left panel shows the energy dependence of the precipitation rate $\nu(E)$. (a)–(c) Model electron numbers at different energies evolving under the transport effect described by $\nu(E)$, which we refer to as weak, intermediate, and strong scattering, respectively. (d) Model fit to the observed microwave light curves at three frequencies. (e) Model fit to the observed microwave spectral index. The inset in (e) shows the evolution of electron energy spectrum used for the fitting. In (a)–(c), t represents time in the model, and in (d) and (e) t represents time after 23:06 UT. The fit is made at a very small loss cone $\alpha_0 \approx 4.3^\circ$ and a large loop, $l \approx 1.4 \times 10^5$ km. (From Lee *et al.* 2002)

region lying on the limb and is brightest at the loop top. By comparing this 34 GHz intensity with the 17 GHz intensity, this loop-top source is found to be clearly optically thin, and therefore must represent an actual confinement of electrons. A concentration of electrons around the loop top may result from magnetic mirroring. However, Melnikov, Shibasaki & Reznikova (2002) have found that magnetic mirroring alone is insufficient to overcome the increase of MWR toward the footpoints due to field strength (see also Petrosian 1982).

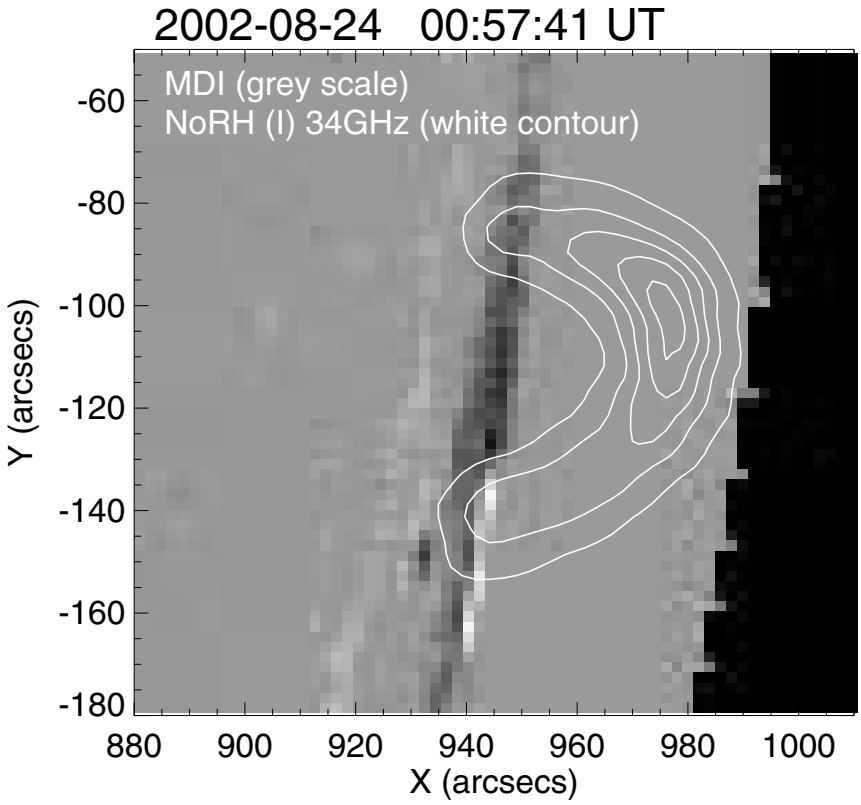

Figure 9.7. A loop top source near the solar limb observed with NoRH at 34 GHz. This MWR source (contours) is found to be optically thin, and therefore represents electrons that are highly concentrated at the loop top. The black and white pixels represent the longitudinal magnetic fields in the active region which lies on the very limb. (From Melnikov, Shibasaki & Reznikova 2003)

Melnikov *et al.* (2002) suggested two possibilities for such local confinement of electrons: either electrons are preferentially accelerated with a perpendicular momentum distribution or the loss of electrons is enhanced at the lower part of the loop. We here consider a third, ad hoc possibility that turbulence leads to strong diffusion and thus the associated trapping is itself localized to the loop top.

4.4 Pitch angle scattering and MWR maps

Each of the above three regimes of pitch angle scattering involve different physics, and it is likely that we can distinguish them in imaging MWR observations. Melrose & White (1979) predicted that, under weak diffusion, asymmetric double peaks will appear on an inhomogeneous magnetic loop (Fig. 9.5), whereas, under intermediate diffusion, electrons are able to access all part of the loop and thus will result in symmetric footpoint emissions. As seen above, electrons can be confined to a localized region under the strong diffusion (Fig. 9.7).

We also expect that the MWR source may move at a speed much slower than the individual particle themselves, so that it can be observable as a moving MWR source. Under the weak diffusion a source may expand toward the footpoints as electrons initially at a restricted range of pitch angles scatter to smaller pitch angles. Under strong diffusion, the electron confinement can expand more rapidly. For instance, Yokoyama *et al.* (2002) observed MWR sources propagating at speed up to $\sim 10^4$ km s^{-1} using the NoRH, which might represent the expansion of a Whistler turbulent region at its phase velocity (Stepanov *et al.* 2003). No actual motion of the microwave source is expected for intermediate diffusion. However we can expect an apparent motion of MWR sources from the loop-top to footpoints in the case where the entire loop is initially optically thick at the maximum phase and becomes optically thin later.

The key diagnostic comes from the spatially resolved MWR spectrum, which we have shown is sensitive to the pitch angle distribution (see Lee & Gary 2000). Nevertheless such investigations are not common for a couple of reasons. First, allowing an evolving pitch angle distribution introduces a number of parameters into calculation of MWR spectrum, which already depends on many largely unknown ambient plasma and accelerated electron parameters. Second, it has been expected that electrons with an anisotropic distribution will be unstable to various instabilities by which they become isotropized quickly (Melrose 1980). Recently, Fleishman & Melnikov (2003ab) addressed this problem by first showing that electrons in an anisotropic pitch angle distribution can be stable against the Cyclotron instablity over a wide range of parameters, although other instabilities are yet to be investigated. In their result, the gyrosynchrotron MWR spectrum from electrons with anisotropic pitch angle and single power-law energy distribution is steeper than that for isotropic electrons (see also Lee & Gary 2000), and furthermore the microwave spectral index itself varies with frequency, unlike the isotropic case. Such spectral diagnostics for anisotropic distributions of electrons may be utilized (and indeed may be necessary) when spatially resolved MWR spectra along a loop become available (e.g. with FASR).

5. Electron Energy Variation

Finally we discuss changes in electron energy during acceleration and transport, which is the main effect that has received attention in the interpretation of both MWR and HXR spectra. To study acceleration using the MWR spectrum, Moghaddam-Taaheri & Goertz (1990) modeled the runaway electrons in the electric field and subsequent pitch angle scattering by turbulence, and compared the predicted MWR spectral evolution with an observation by Marsh *et al.* (1981). Benka & Holman (1992) used a combination of thermal and nonthermal electrons in a model in which a DC field variation results in a typical OVSA spectral variation (Stähli, Gary & Hurford 1990). This acceleration process, in our formulations, amounts to determining $Q(E,t)$. On the other hand, the transport study is usually made assuming a time invariant injection spectrum, $Q(E,t) = q(E)T(t)$ and all spectral changes in the decay are attributed to the energy dependence of ν. The top panels in Figure 9.6 show some examples of such attempts. In many transport studies, efforts are made to confirm that $\nu(E)$ inferred from observations is consistent with the Coulomb collision physics. Such studies have provided some understanding of time delay, spectral hardening, etc. A recent comprehensive study using OVSA spectral data has been made by Melnikov & Silva (1999; 2000) and Silva *et al.* (2000).

Note that not all of these studies on energy dependent processes in phase space employ the trap-and-precipitation paradigm, in spite of the ample evidence for this hypothesis. It will thus be worthwhile to discuss how the paradigm will change once this trap-and-precipitation system is introduced.

1. Time delay and spectral hardening of MWR with respect to HXR are often attributed to the energy dependence of Coulomb collisions. However, the trapped component will always show time delay with respect to the directly precipitating electrons regardless of the scattering mechanism (see top panels of Fig. 9.6). The harder electron distribution in a trap is also possible for other reasons not entirely due to Coulomb collisions. For instance, Lee & Gary (1994) feed a common Whistler turbulence into two regions with weak and strong magnetic fields, which are assumed for MWR and HXR emitting regions, respectively, and find a steeper energy spectrum in the latter region due to the enhanced escape rate there. See also the discussion made in §3.2 for two different values of ν for MWR and HXR. It should therefore be clarified whether the relative differences of MWR and HXR time profiles arise solely due to the energy dependence of the radiations or due to the different conditions in the trap-and-precipitation regions.

2. If the Razin effect, suppression of radiation due to ambient plasma (Ramaty 1969), is observed together with the spectral flattening (cf. Belkora

1997), this may provide additional evidence for the importance of Coulomb collisions.

3. Some studies indicated that the trap region contains higher energy electrons and precipitation is primarily by lower energy electrons. This is consistent with the physics of Coulomb collisions. However, one can be misled by the radiative characteristics of MWR. Even though electrons in the entire energy range are equally trapped and precipitating, the coronal trap has weaker magnetic field and thus emits MWR at higher harmonics. As a result, the loop-top MWR represents relatively higher energy electrons at a given frequency. On the other hand, the precipitating region has stong magnetic field and the MWR from the region is dominated by low harmonics and thus correspondingly low energy electrons (cf. Kosugi *et al.* 1988). It is therefore essential to take into account the ambient magnetic field strength in relating the MWR frequency to electron energy.

4. In some studies, time correlation of MWR and HXR fluxes has been investigated to determine the energy of electrons that contribute most to a given frequency. Note however that the electrons staying in the trap would have a more extended life than the precipitating electrons, even though injected at the same time and energy. The magnetic trap thus acts as a machine to separate the two populations in time as well as in space. Accordingly, such correlation of the two radiations at a fixed time interval may be misleading in the presence of the magnetic trapping.

5. MWR has both optically thick and thin parts, each of which responds to injection spectrum very differently. While a thin MWR flux varies in proportion to the number of electrons like HXR, optically thick MWR represents a mean energy or effective temperature. For instance, if the emitting electrons are nonthermal in a single power-law distribution with index δ, the optically-thick MWR directly responds to δ avoiding confusion with the increase in N (see simplified expression for the effective temperature by Dulk & Marsh 1984). Accordingly, the optically thick MWR is rather important when the injection spectrum changes with time, which has often been ignored in the transport problem. In this case the structure of trap-and-precipitation is important, because direct precipitation is more likely to be optically thick as electrons pass through the strongest fields (see Fig. 8 of Lee *et al.* 2002).

6. Concluding Remarks

In this chapter, we have discussed MWR as an important clue to understand electron kinetic processes occurring in solar flares. Our emphasis was on the trap-and-precipitation paradigm, which naturally arises in the presence of in-

homogeneous magnetic fields on the Sun and is responsible for the relative differences between MWR and HXR. It is this framework that we take as a means to distinguish the acceleration from the transport, which is otherwise a difficult deconvolution problem. The pitch angle and energy variation have also been discussed within this framework, which puts us in a better position to derive physical properties of the acceleration and transport mechanisms.

Based on the ideas discussed in this chapter, we briefly comment on the traditionally suggested utility of MWR in the study of solar flares. MWR has often been regarded as appropriate for trapped electrons while HXR relate more to acceleration (Melnikov 1994). We found that the MWR well represents the trapped electrons because of its greater sensitivity to energetic electrons in the absence of cooler ambient plasma. We have shown that this sensitivity can be used, on the contrary, to derive information on the acceleration properties. To summarize: (1) MWR helps to locate those electrons produced in the high tenuous corona that are not precipitating into lower atmosphere and therefore are largely undetected by HXR and other lower energy radiations. (2) In some events, the slowly evolving nature of trapped electrons as measured in MWR allows us to investigate injection properties, within the instrumental time resolution. (3) The field strength dependence of MWR provides a strong constraint on the electron spatial distribution on a magnetic loop. (4) MWR spectra have both optically thick and thin emission, which provides diagnostics on N and δ, respectively. This is particularly useful when the acceleration spectrum changes with time. There has been a concern that inversion of MWR to flare parameters is more complicated than that of HXR, as it involves many parameters (Gary 2000). We however recognize that this complexity arises from two major ingredients in the electron transport problem: the magnetic field and electron pitch angles. We therefore suggest that future advance in MWR study would depend on how well we can use MWR observations to address the pitch angle and magnetic fields.

Until now, the diagnostics discussed in this chapter have not been fully exploited, largely due to the absence of high spatial and spectral resolution imaging spectroscopy. The ideas about trapping were proposed some time ago (Melnikov 1990; 1994), but the identification of direct precipitation in MWR was begun only recently (Kundu *et al.* 2001*a*; Lee *et al.* 2002). Imaging and spectral MWR observations for the study of pitch angle diffusion and associated acceleration properties is just beginning (Lee & Gary 2000; Melnikov *et al.* 2002; 2003). A topic that is closely related to the present context but not discussed here is the MWR study for multi-loop interactions (Hanaoka 1996; 1997; Nishio *et al.* 1994; 1997; Kundu *et al.* 2001*b*). This has direct implications for magnetic reconnection (see also Kundu *et al.* 1982*ab*), and therefore is significant in relating the electron kinetics to solar flare magnetohydrodynamics. Electron

propagation in a magnetic reconnection region may be handled by extending the present paradigm to a multiple system of trap-and-precipitation (Aschwanden *et al.* 1999). Currently the effort to achieve these goals is shared by OVSA with spectral capabilities and the VLA and Nobeyama Radioheliograph with imaging capability. The FASR, as an instrument targeted to this spectral imaging capability, will therefore not only integrate all the currently available knowledge but also achieve a new level of MWR study to advance our knowledge of kinetic processes during solar flares.

References

Alissandrakis, C. E. & Preka-papadema, P. 1984, A&A, 139, 507
Aschwanden, M. J. 2003, Particle Acceleration and Kinematics in Solar Flares, Reprinted from SPACE SCIENCE REVIEWS, Volume 101, Nos. 1-2, Kluwer Academic Publishers, Dordrecht
Aschwanden, M. J. 1998, ApJ, 502, 455
Aschwanden, M. J., Bynum, R. T., Kosugi, T., Hudson, H., and Schwartz, R.A. 1997, ApJ, 487, 936
Aschwanden, M. J., & Alexander, D. 2001 Solar Phys, 204, 93
Aschwanden, M. J., Schwartz, R. A., & Dennis, B. R. 1998, ApJ, 502, 468
Aschwanden, M. J., Kosugi, T., Hanaoka, Y., Nishio, M., & Melrose, D. B. 1999, ApJ, 526, 1026
Bai, T. & Ramaty, R. 1979, ApJ, 227, 1072
Bai, T. 1986, ApJ, 308, 912
Bastian, T. S. & Aschwanden, M. J. 1997, BAAS, Vol. 29, p.922
Bastian, T. S., Benz, A. O., & Gary, D. E. 1998, ARAA, 36, 131
Belkora, L. 1997, ApJ, 481, 582
Benka, S. G. & Holman, G. D.: 1992, ApJ, 391, 854
Bespalov, P. A., Zaitsev, V. V., & Stepanov, A. V. 1991, ApJ, 374, 369
Brown, J. C., Conway, A. J., & Aschwanden, M. J. 1998, ApJ, 509, 911
Bruggmann, G., Vilmer, N., Klein, K.-L., & Kane, S. R.: 1994, Solar Phys, 149, 171
Cornell, M. E., Hurford, G. J., Kiplinger, A. L., & Dennis, B. R. 1984, ApJ, 279, 875
Crannell, C. J., Frost, K. J., Saba, J. L., Maetzler, C. & Ohki, K. 1978, ApJ, 223, 620
Daibog, E. I., Mel'Nikov, V. F., Stolpovskii, V. G. 1993, Solar Phys, 144, 361
Daibog, E. I., Stolpovskii, V. G., Melnikov, V. F., Podstrigach, T. S. 1989, Soviet Astr.Lett.(Tr:PISMA) V.15, NO. 6/NOV, 432
Dulk, G. A. 1985, ARAA, 23, 169
Dulk, G. A. & Marsh, K. A. 1982, ApJ, 259, 350
Fleishman, G. D. & Melnikov, V. F. 2003a, ApJ, 584, 1071

Fleishman, G. D. & Melnikov, V. F. 2003*b*, ApJ, 587, 823
Gary, D. E. 2000, in High Energy Solar Physics-Anticipating HESSI, ASP Conf. Ser. 206, 297
Ginzburg, V. L. & Syrovatskii, S. I. 1965, ARAA, 3, 297
Hanaoka, Y. 1997, Solar Phys, 173, 319
Hanaoka, Y. 1996, Solar Phys, 165, 275
Holman, G. D., Kundu, M. R., & Papadopoulos, P. 1982, ApJ, 257, 354
Kai., K. 1986, Solar Phys, 104, 235
Kai, K. Kosugi, T., & Nitta, N. 1985, PASP, 37, 155
Kennel, C. F. 1969, Rev. Geophys. Space Phys., 7, 379
Klein, K.-L., Trottet, G., & Magun, A. 1986, Solar Phys. 104, 243
Klein, K.-L. & Trottet, G. 1984, A&A, 141, 67
Kosugi, T., Dennis, B. R., & Kai, K. 1988, ApJ, 324, 1118
Kundu, M. R., White, S. M., Shibasaki, K., Sakurai, T., & Grechnev, V. V. 2001*a*, ApJ, 547, 1090
Kundu, M. R., Grechnev, V. V., Garaimov, V. I., & White, S. M. 2001*b*, ApJ, 563, 389
Kundu, M. R., Nitta, N., White, S. M., Shibasaki, K., Enome, S., Sakao, T., Kosugi, T., & Sakurai, T. 1995, ApJ, 454, 522
Kundu, M. R., Schmahl, E. J., Vlahos, L., & Velusamy, T. 1982b, A&A, 108, 188
Kundu, M. R., Schmahl, E. J., & Velusamy, T. 1982a, ApJ, 253, 963
Lee, J., Gallagher, P. T., Gary, D. E., Nita, G. M., Choe, G. S., Bong, S.-C., & Yun, H. S. 2003, ApJ, 585, 524
Lee, J. & Gary, D. E. 1994, Solar Phys, 153, 347
Lee, J., Gary, D. E., & Zirin, H. 1994, Solar Phys, 152, 409
Lee, J., Gary, D. E., & Shibasaki, K. 2000, ApJ, 531, 1109
Lee, J. & Gary, D. E. 2000, ApJ, 543, 457
Lee, J., Gary, D. E., Qiu, J., & Gallagher, P. T. 2002, ApJ, 572, 609
Lu, E. T. and Petrosian, V. 1988, ApJ, 327, 405
MacKinnon, A. L. 1991, A&A, 242, 256
Marsh, K. A., Hurford, G. J., Zirin, H., Dulk, G. A., Dennis, B. R., Frost, K. J., & Orwig, L. E. 1981, ApJ, 251, 797
Marsh, K. A. & Hurford, G. J., 1982, ARAA, 20, 497
Marsh, K. A. & Hurford, G. J., 1980, ApJ, 240, L111
Masuda, S., Kosugi, T., Hara, H., Tsuneta, S., & Ogawara, Y. 1994 Nature, 371, 495
Melnikov, V. F. 1990, Ph.D. Thesis, Radiophysical ResearchInstitute, Nizhniy Novgorod, Russia
Melnikov, V. F., Podstrigach, T. S., Daibog, E. I., Stolpovskii, V. G. 1991, CosRe 29, 95
Melnikov, V. F. 1994, Radiophys. Quant. Electron. 37, 557

Melnikov, V. F. & Magun, A. 1998 Solar Phys, 178, 153
Melnikov, V. F., Shibasaki, K., & Reznikova, V. E. 2002, ApJ, 580, L185
Melnikov, V. F., Shibasaki, K., & Reznikova, V. E. 2003, ApJ, in preparation
Melnikov, V. F. & Silva, A. V. R. 1999, Ninth European Meeting on Solar Physics: Magnetic Fields and Solar Processes. Florence, Italy, 12-18 September, 1999. Proceedings published in ESA SP Series (SP-448), ed. A. Wilson.
Melnikov, V. F. & Silva, A. V. R. 2000, in High Energy Solar Physics-Anticipating HESSI, ASP Conf. Ser. 206, 371
Melrose, D. B. 1980, Plasma Astrophysics, (New York: Gordon and Breach)
Melrose, D. B. & Brown, J. C. 1976, MNRAS, 176, 15
Melrose, D. B. & White, S. M. 1979, Proc Astron. Soc. Australia, 3, 369
Moghaddam-Taaheri, E. & Goertz, C. K. 1990, ApJ, 352, 361
Miller, J. A., Cargill, P. J., Emslie, A. G., Holman, G. D., Dennis, B. R., LaRosa, T. N., Winglee, R. M., Benka, S. G., & Tsuneta, S. 1997, JGR, 102, 14631
Nishio, M., *et al.* 1994 PASJ 46, L11
Nishio, M., Yaji, K., Kosugi, T., Nakajima, H., & Sakurai, T. 1997, ApJ, 489, 976
Petrosian, V. 1990, in Basic plasma processes on the sun (A92-30901 12-92). Dordrecht, Netherlands, Kluwer Academic Publishers, p. 391
Petrosian, V. 1982, ApJ, 255, L85
Petrosian, V. 1981, ApJ, 251, 727
Preka-Papadema, P., & Alissandrakis, C. E. 1992, A&A, 257, 307
Ramaty, R. 1969, ApJ, 158, 753
Sakao, T. 1994, Ph.D. thesis, University of Tokyo
Silva, A. V. R., Wang, H., & Gary, D. E. 2000, ApJ, 545, 1116
Spitzer, L. 1967, The Physics of Fully Ionized Gases (2d ed., New York: Interscience)
Stähli, M., Gary, D. E., & Hurford, G. J. 1990, Solar Phys., 125, 343.
Stepanov, A. V., Melnikov, V. F., Yokoyama, T., Nakajima, H., & Shibasaki, K. 2003, in preparation
Takakura, T. & Kai. K. 1966, PASJ 18, 57
Trottet, G. & Vilmer, N. 1984, Adv. in Space Res. 4 (2-3), 153
Trubnikov, B. A. 1965, Rev. Plasma Phys., 1, 105
Vilmer, N., Kane, S. R., & Trottet, G. 1982, A&A, 108, 306
Yokoyama, T., Nakajima, H., Shibasaki, K., Melnikov, V. F., & Stepanov, A. V. 2002, ApJ, 576, L87
Wild, J.P. & Smerd, S.F. 1972, ARAA, 10, 159